IN THE UNITED STATES PATENT AND TRADEMARK OFFICE

In re application of: Cunningham et al.	Attorney Docket No.: STUFP155/S03-185
Application No.: 10/823,979	Examiner: Vargas, Dixomara
Filed: April 13, 2004	Group: 2859
Title: NON-LINEAR SYMMETRIC SWEEP SPECTRAL-SPATIAL RF PULSES FOR MR SPECTROSCOPY	Confirmation No.: 5327

DECLARATION UNDER 37 CFR § 1.132

Commissioner for Patents
P.O. Box 1450
Alexandria, VA 22313-1450

Sir:

We, Charles H. Cunningham, John M. Pauly and Daniel B. Vigneron, declare as follows:

1. We are the applicants in the above-identified patent application.

2. We are co-authors along with Albert P. Chen, Duan Xu, Ralph E. Hurd, and Napapon Sailasuta of "Design of Symmetric-Sweep Spectral-Spatial RF Pulses for Spectral Editing", Magnetic Resource in Medicine 2004 July; 52(1):147-153; and are co-authors along with Ralph E. Hurd and Napapon Sailasuta of "Design of Symmetric-Sweep Spectral-Spatial RF Pulses for Spectral Editing", Department of Electrical Engineering, Stanford University, October 2003.

3. To the extent that either of the papers identified above disclose the invention described and claimed in said patent application, the disclosure is attributable solely to us and not to other co-authors.

4. We hereby declare that all statements made herein of our own knowledge are true and that all statements made on information and belief are believed to be true. We further declare that these statements are made with the knowledge that willful false statements and the like so made are punishable by fine or imprisonment, or both (under Section 1001 of Title 18 of

the United States Code), and that such willful false statements may jeopardize the validity of the application or any patent issued thereon.

Charles H. Cunningham

6/15/2005
Date

John M. Pauly

6/15/2005
Date

Daniel B. Vigneron

Date

IN THE UNITED STATES PATENT AND TRADEMARK OFFICE

In re application of: Cunningham et al.	Attorney Docket No.: STUFP155/S03-185
Application No.: 10/823,979	Examiner: Vargas, Dixomara
Filed: April 13, 2004	Group: 2859
Title: NON-LINEAR SYMMETRIC SWEEP SPECTRAL-SPATIAL RF PULSES FOR MR SPECTROSCOPY	Confirmation No.: 5327

DECLARATION UNDER 37 CFR § 1.132

Commissioner for Patents
P.O. Box 1450
Alexandria, VA 22313-1450

Sir:

We, Charles H. Cunningham, John M. Pauly and Daniel B. Vigneron, declare as follows:

1. We are the applicants in the above-identified patent application.

2. We are co-authors along with Albert P. Chen, Duan Xu, Ralph E. Hurd, and Napapon Sailasuta of "Design of Symmetric-Sweep Spectral-Spatial RF Pulses for Spectral Editing", Magnetic Resource in Medicine 2004 July; 52(1):147-153; and are co-authors along with Ralph E. Hurd and Napapon Sailasuta of "Design of Symmetric-Sweep Spectral-Spatial RF Pulses for Spectral Editing", Department of Electrical Engineering, Stanford University, October 2003.

3. To the extent that either of the papers identified above disclose the invention described and claimed in said patent application, the disclosure is attributable solely to us and not to other co-authors.

4. We hereby declare that all statements made herein of our own knowledge are true and that all statements made on information and belief are believed to be true. We further declare that these statements are made with the knowledge that willful false statements and the like so made are punishable by fine or imprisonment, or both (under Section 1001 of Title 18 of

the United States Code), and that such willful false statements may jeopardize the validity of the application or any patent issued thereon.

Charles H. Cunningham

Date

John M. Pauly

Date

Daniel B. Vigneron

6/2/05

Date

Parameter Relations for the Shinnar–Le Roux Selective Excitation Pulse Design Algorithm

John Pauly, *Member, IEEE*, Patrick Le Roux, Dwight Nishimura, *Member, IEEE*, and Albert Macovski, *Fellow, IEEE*

***Abstract*—Selective excitation pulses are used in magnetic resonance imaging (MRI) to isolate a specific slice through the subject. The pulse design problem is in general nonlinear due to the nonlinearity of the Bloch equation. Recently a direct solution has been proposed by Shinnar and his co-workers [1]–[6], and Le Roux [7]–[9].**

In this paper we first present an overview of the Shinnar–Le Roux (SLR) algorithm. We then show how the performance of SLR pulses can be very accurately specified analytically. This is useful because it tells how to design a pulse that produces a specified slice profile. More importantly, it allows the pulse designer to trade-off analytically the parameters describing the pulse performance. We present several examples to illustrate the more important trade-offs. These include linear-phase and minimum- and maximum-phase pulses. Linear-phase pulses can be refocused with a gradient reversal, and can be used as spin-echo pulses. Minimum- and maximum-phase pulses have better slice profiles, but cannot be completely refocused.

I. Introduction

MAGNETIC resonance imaging (MRI) is inherently a volume imaging modality. Spatially selective RF pulses restrict this volume to a thin slab of material, which can then be resolved in the two remaining directions to produce a two-dimensional image. The RF pulse design problem is in general nonlinear due to the nonlinearity of the Bloch equation. For small-tip-angle pulses a Fourier analysis can be used [10], [11]. These pulses continue to perform reasonably well for tip angles on the order of $\pi/2$. Better $\pi/2$ pulses can be designed using optimization methods. For tip angles of π, optimized pulses are essential for good slice profiles [12]–[16].

Recently a new method for slice selective pulse design has been proposed independently by Shinnar and his co-workers [1]–[6], and Le Roux [7]–[9]. It is based on a discrete approximation to the spin domain version of the Bloch equation. The RF pulse design problem can then be mapped into a digital filter design problem, which can be solved using well-known algorithms. The resulting digital filter is then mapped back into an RF pulse.

In the first part of the paper we present a brief overview of the Shinnar–Le Roux (SLR) algorithm. Enough detail is presented to allow the reader to implement the algorithm.

The main part of the paper concerns the specification of the slice profile produced by an SLR pulse. Simple analytic expressions relate the transition width, in-slice ripple, out-of-slice ripple, and time–bandwidth product. These relationships also show how to design a pulse that achieves the predicted theoretical performance. Previously pulse sequences had to be designed around available RF pulses. Now RF pulse design can be an integral part of pulse sequence design.

To illustrate the nature of the slice profile trade-offs we present several pulse design examples. The case of a slice-selective $\pi/2$ pulse is considered in some detail. Then examples illustrating the design of inversion, spin-echo, and saturation pulses are presented.

These examples include both linear-phase, and minimum- and maximum-phase pulses. A linear-phase $\pi/2$ pulse can be refocused with a gradient reversal, and a linear-phase π pulse can be used as a spin-echo pulse. The additional constraint of requiring linear phase has a cost in slice profile. If this constraint is eliminated better slice-profiles can be obtained. We present examples of minimum-phase and maximum-phase (reversed minimum-phase) pulses that have significantly better slice profiles than the corresponding linear-phase pulses. These are useful when slice-profile phase is unimportant, such as inversion or saturation pulses.

II. The Shinnar–Le Roux Algorithm

The Bloch equation reduces to a rotation if relaxation effects are neglected. The solution to the Bloch equation is then the initial magnetization multiplied by a 3×3 orthonormal matrix. This rotation can also be represented by a 2×2 unitary matrix, the so-called spin-domain representation. The SLR algorithm is based on a discrete approximation to the spin domain version of the Bloch equation. This further simplifies the solution of the Bloch equation to the design of two polynomials. RF pulse design becomes a polynomial design problem, which can be solved using well-known digital filter design algorithms.

A. Spin Domain Bloch Equation

The Bloch equation, neglecting relaxation, is given by

$$\begin{pmatrix} \dot{M}_x \\ \dot{M}_y \\ \dot{M}_z \end{pmatrix} = \gamma \begin{pmatrix} 0 & Gx & -B_{1,y} \\ -Gx & 0 & B_{1,x} \\ B_{1,y} & -B_{1,x} & 0 \end{pmatrix} \begin{pmatrix} M_x \\ M_y \\ M_z \end{pmatrix}$$

where $B_1 = B_{1,x} + iB_{1,y}$ is the applied time varying RF field, and G is the gradient amplitude. The gradient is assumed to lie along the $+x$ axis. The solution to this equation is a rotation

$$M(T) = RM(0)$$

where R is a 3×3 orthonormal matrix. If a sequence of n pulses has been applied, the solution is the product of the in-

Manuscript received May 18, 1990; revised October 9, 1990. This work was supported by the GE Medical Systems Group under Grant 22-84, by the National Institutes of Health under Grant HL 34962, and by the National Science Foundation under Contract ECS 88-01798.

J. Pauly, D. Nishimura, and A. Macovski are with the Information Systems Laboratory, Stanford University, Stanford, CA 94305.

P. Le Roux is with the GE Medical Systems Group, Milwaukee, WI 53188.

IEEE Log Number 9041389.

0278-0062/91/0300-0053$01.00 © 1991 IEEE

dividual rotations R_i

$$R = R_n R_{n-1} \cdots R_1.$$

These rotations can also be represented by 2 × 2 unitary matrices

$$Q = \begin{pmatrix} \alpha & -\beta^* \\ \beta & \alpha^* \end{pmatrix}$$

where α and β are the Cayley-Klein parameters

$$\alpha = \cos \phi/2 - in_z \sin \phi/2 \quad (1)$$

$$\beta = -i(n_x + in_y) \sin \phi/2. \quad (2)$$

The vector n is the axis of the rotation and ϕ is the rotation angle. These spin matrices multiply just as the 3 × 3 matrices do. The Cayley-Klein parameters satisfy the constraint

$$\alpha\alpha^* + \beta\beta^* = 1. \quad (3)$$

The spin matrices can be used to calculate the effect of an RF pulse in the presence of a constant gradient. We assume that the RF is piece-wise constant (illustrated in Fig. 1). This is a good approximation to the way that RF waveforms are generated on commercial imaging systems. If the jth RF sample has a complex amplitude $B_{1,j}$ and a duration Δt, the rotation parameters are

$$\phi_j = -\gamma \Delta t \sqrt{|B_{1,j}|^2 + (Gx)^2}$$

$$n_j = \frac{\gamma \Delta t}{|\phi_j|} (B_{1,x,j}, B_{1,y,j}, Gx).$$

The Cayley-Klein parameters for the jth interval are then

$$a_j = \cos \phi_j/2 - in_{z,j} \sin \phi_j/2$$

$$b_j = -i(n_{x,j} + in_{y,j}) \sin \phi_j/2.$$

The spin-domain rotation matrix is then

$$Q_j = \begin{pmatrix} a_j & -b_j^* \\ b_j & a_j^* \end{pmatrix}$$

and the total rotation produced by the pulse is

$$Q = Q_n Q_{n-1} \cdots Q_1. \quad (4)$$

Given the spin-domain representation of the rotation produced by a pulse, we can calculate the 3 × 3 rotation matrix by inverting the expressions for the Cayley-Klein parameters. Usually, though, the quantity of interest is the magnetization produced given some initial condition. These are calculated easily using the expression (adapted from [17])

$$\begin{pmatrix} M_{xy}^+ \\ M_{xy}^{+*} \\ M_z^+ \end{pmatrix} = \begin{pmatrix} (\alpha^*)^2 & -\beta^2 & 2\alpha^*\beta \\ -(\beta^*)^2 & \alpha^2 & 2\alpha\beta^* \\ -\alpha^*\beta^* & -\alpha\beta & \alpha\alpha^* - \beta\beta^* \end{pmatrix} \begin{pmatrix} M_{xy}^- \\ M_{xy}^{-*} \\ M_z^- \end{pmatrix}$$

where $M_{xy} = M_x + iM_y$.

There are a number of useful special cases. If the initial magnetization is the equilibrium magnetization $M^- = (0, 0, M_0)^T$, the excitation slice profile is

$$M_{xy}^+ = 2\alpha^*\beta M_0 \quad (5)$$

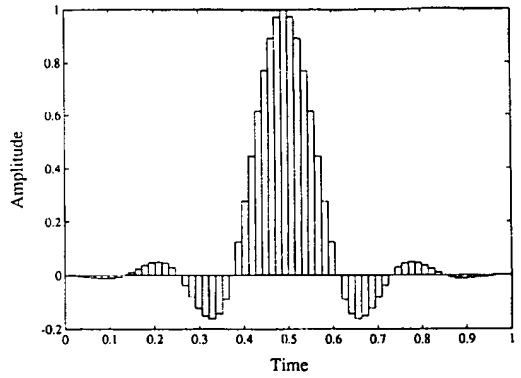

Fig. 1. Piece-wise constant RF. This is a good approximation to the way RF waveforms are generated on commercial imagers.

and the inversion slice profile is

$$M_z^+ = (\alpha\alpha^* - \beta\beta^*)M_0. \quad (6)$$

For the spin-echo profile the initial magnetization is $M^- = (M_{xy}^-, M_{xy}^{-*}, 0)^T$. The spin-echo profile is then

$$M_{xy}^+ = (\alpha^*)^2 M_{xy}^- - \beta^2 M_{xy}^{-*}. \quad (7)$$

If the initial magnetization is along the $+y$ axis, this becomes

$$M_{xy}^+ = i((\alpha^*)^2 + (\beta)^2)M_0. \quad (8)$$

A case of considerable practical interest is of a spin-echo pulse surrounded by crusher gradients. The crusher gradients suppress the parasitic FID's produced by the slice profile transition regions. A single crusher gradient produces a rotation about the z axis of

$$\phi(x) = -x\left\{\gamma \int G(t)\, dt\right\}.$$

The spin-domain rotation matrix for this rotation is

$$R_c = \begin{pmatrix} e^{-i\phi(x)/2} & 0 \\ 0 & e^{i\phi(x)/2} \end{pmatrix}.$$

The rotation produced by the spin-echo pulse surrounded by crusher gradients is

$$R_c R R_c = \begin{pmatrix} \alpha e^{-i\phi(x)} & -\beta^* \\ \beta & \alpha^* e^{i\phi(x)} \end{pmatrix}.$$

The spin-echo pulse profile from (7) is

$$M_{xy}^+ = (\alpha^*)^2 e^{i2\phi(x)} M_{xy}^- - (\beta)^2 M_{xy}^{-*}.$$

The crusher gradient leaves a large number of cycles of phase twist across an imaged voxel. If we integrate over a voxel the first term integrates to zero, leaving

$$M_{xy}^+ = -\beta^2 M_{xy}^{-*}. \quad (9)$$

Again, if the initial magnetization was along the $+y$ axis, the final magnetization produced by the crushed spin-echo pulse is

$$M_{xy}^+ = i\beta^2 M_0. \quad (10)$$

Once the Cayley-Klein parameters have been determined for a selective excitation pulse it is easy to calculate any profile of

interest. The spin domain description is an extremely convenient representation for selective excitation pulses.

B. State-Space Description of Spin-Domain Rotations

The result of an RF pulse applied in the presence of a constant gradient field can be calculated by multiplying 2×2 unitary matrices, as in (4). This matrix product has considerable redundancy due to the symmetry of the spin-matrices, allowing an even simpler representation. The state of the rotation at a given point in the pulse sequence may be represented by a 2×1 complex vector. The matrix-matrix products are replaced by matrix-vector products.

If we write out the sequence of matrix products of (4)

$$\begin{pmatrix} \alpha_n & -\beta_n^* \\ \beta_n & \alpha_n^* \end{pmatrix} = \begin{pmatrix} a_n & -b_n^* \\ b_n & a_n^* \end{pmatrix} \cdots \underbrace{\begin{pmatrix} a_j & -b_j^* \\ b_j & a_j^* \end{pmatrix} \cdots \begin{pmatrix} a_0 & -b_0^* \\ b_0 & a_0^* \end{pmatrix}}_{\begin{pmatrix} \alpha_j & -\beta_j^* \\ \beta_j & \alpha_j^* \end{pmatrix}}.$$

Multiplication of the matrices up to j produces the rotation Q_j. From the structure of Q_j it is apparent that two of the four entries are redundant. The same information can be represented by either column of the rotation matrix. We will choose the first column, $(\alpha_j\ \beta_j)^T$. The effect of the pulse may then be calculated by propagating this vector

$$\begin{pmatrix} \alpha_j \\ \beta_j \end{pmatrix} = \begin{pmatrix} a_j & -b_j^* \\ b_j & a_j^* \end{pmatrix} \begin{pmatrix} \alpha_{j-1} \\ \beta_{j-1} \end{pmatrix}.$$

This is a state-space description of the RF pulse. Since the initial state is no rotation, the initial condition can be found by substituting a rotation angle $\phi = 0$ into (1) and (2).

$$\begin{pmatrix} \alpha_0 \\ \beta_0 \end{pmatrix} = \begin{pmatrix} 1 \\ 0 \end{pmatrix}.$$

C. Hard-Pulse Approximation and the Forward SLR Transform

The key step in the development of the SLR algorithm is the so-called hard-pulse approximation [18]. With this approximation the state-space description can be reduced to two polynomials. This mapping of an RF pulse into two complex polynomials we call the forward SLR transform.

During an excitation pulse the magnetization is rotating about the vector sum of the RF field and the local gradient field. The basic idea of the hard-pulse approximation is that if the angle is small the rotation can be modeled by two sequential rotations. The first is free precession under the effect of the local gradient field by an angle $-\gamma G x \Delta t$. The second is the rotation about the applied RF vector by an angle $-\gamma B_1 \Delta t$.

If we write Q_j as the product of the two sequential spin matrices, we get

$$Q_j = \begin{pmatrix} C_j & -S_j^* \\ S_j & C_j \end{pmatrix} \begin{pmatrix} z^{1/2} & 0 \\ 0 & z^{-1/2} \end{pmatrix}$$

where

$$\begin{aligned} C_j &= \cos\left(\gamma |B_{1,j}| \Delta t/2\right) \\ S_j &= i e^{i \angle B_{1,j}} \sin\left(\gamma |B_{1,j}| \Delta t/2\right) \\ z &= e^{i\gamma G x \Delta t}. \end{aligned} \tag{11}$$

The state-space recursion for the Cayley-Klein parameters then becomes

$$\begin{pmatrix} \alpha_j \\ \beta_j \end{pmatrix} = z^{1/2} \begin{pmatrix} C_j & -S_j^* \\ S_j & C_j \end{pmatrix} \begin{pmatrix} 1 & 0 \\ 0 & z^{-1} \end{pmatrix} \begin{pmatrix} \alpha_{j-1} \\ \beta_{j-1} \end{pmatrix}.$$

Defining

$$\begin{aligned} A_j &= z^{j/2} \alpha_j \\ B_j &= z^{j/2} \beta_j \end{aligned} \tag{12}$$

the recursion may be reduced to

$$\begin{aligned} \begin{pmatrix} A_j \\ B_j \end{pmatrix} &= \begin{pmatrix} C_j & -S_j^* \\ S_j & C_j \end{pmatrix} \begin{pmatrix} 1 & 0 \\ 0 & z^{-1} \end{pmatrix} \begin{pmatrix} A_{j-1} \\ B_{j-1} \end{pmatrix} \\ &= \begin{pmatrix} C_j & -S_j^* z^{-1} \\ S_j & C_j z^{-1} \end{pmatrix} \begin{pmatrix} A_{j-1} \\ B_{j-1} \end{pmatrix}. \end{aligned} \tag{13}$$

Given that $A_0 = \alpha_0 = 1$ and $B_0 = \beta_0 = 0$, the first two states are

$$\begin{pmatrix} A_1 \\ B_1 \end{pmatrix} = \begin{pmatrix} C_1 \\ S_1 \end{pmatrix}$$

$$\begin{pmatrix} A_2 \\ B_2 \end{pmatrix} = \begin{pmatrix} C_2 C_1 - S_2^* S_1 z^{-1} \\ S_2 C_1 + C_2 S_1 z^{-1} \end{pmatrix}.$$

The Cayley-Klein parameters at the nth time step are $(n-1)$ order polynomials in z^{-1}

$$A_n(z) = \sum_{j=0}^{n-1} a_j z^{-j}$$

$$B_n(z) = \sum_{j=0}^{n-1} b_j z^{-j}$$

where

$$z^{-1} = e^{-i\gamma G x \Delta t}.$$

The representation of the rotation produced by a selective excitation pulse has been reduced from a product of n 3×3 matrices to two $(n-1)$-order polynomials.

The recursion given in (13) with the coefficients given in (11) maps an RF pulse $B_1(t)$ into two complex polynomials $A_n(z)$ and $B_n(z)$. This mapping is the forward SLR transform. In the small-tip-angle case the SLR transform reduces to the familiar z-transform.

D. Inverse SLR Transform

Given two related polynomials $A_n(z)$ and $B_n(z)$, the SLR transform can be inverted to calculate the RF pulse that produces these polynomials. This is called the inverse SLR transform. It is this inverse transform that reduces RF pulse design to polynomial design.

The two $(n-1)$ order polynomials $A_n(z)$ and $B_n(z)$ must

satisfy the frequency response (slice profile) amplitude constraint

$$|A_n(z)|^2 + |B_n(z)|^2 = 1 \tag{14}$$

for all complex z such that $|z| = 1$. This is (3) with the substitutions indicated by (12). With this constraint the two polynomials $A_n(z)$ and $B_n(z)$ are valid representations of a rotation at any position x and $z = e^{i\gamma Gx\Delta t}$.

The inverse SLR transform is found by the inversion of the state-space recursion. The forward recursion is

$$\begin{pmatrix} A_j \\ B_j \end{pmatrix} = \begin{pmatrix} C_j & -S_j^* z^{-1} \\ S_j & C_j z^{-1} \end{pmatrix} \begin{pmatrix} A_{j-1} \\ B_{j-1} \end{pmatrix}.$$

The inverse recursion is found by multiplying both sides by the inverse of the incremental rotation matrix, producing

$$\begin{pmatrix} A_{j-1} \\ B_{j-1} \end{pmatrix} = \begin{pmatrix} C_j & S_j^* \\ -S_j z & C_j z \end{pmatrix} \begin{pmatrix} A_j \\ B_j \end{pmatrix} = \begin{pmatrix} C_j A_j + S_j^* B_j \\ z(-S_j A_j + C_j B_j) \end{pmatrix}. \tag{15}$$

Since the incremental rotation and its inverse are both unitary matrices, the constraint of (14) is preserved, and the reduced-order polynomials are also valid representations of a rotation for all $|z| = 1$.

At any stage of the backward recursion we know the coefficients of $A_j(z)$ and $B_j(z)$. Since $A_{j-1}(z)$ and $B_{j-1}(z)$ are lower order polynomials, the leading term in $A_{j-1}(z)$ and the low-order term in $B_{j-1}(z)$ must drop out

$$C_j A_{j,j-1} + S_j^* B_{j,j-1} = 0$$
$$-S_j A_{j,0} + C_j B_{j,0} = 0.$$

These two equations are equivalent, as may be seen by expanding (14) as a polynomial and noting that all except the constant term are zero. The high-order term is

$$A_{j,j-1} A_{j,0}^* + B_{j,j-1} B_{j,0}^* = 0.$$

With this relation either equation may be derived from the other.

Here we choose the second equation to determine the RF. The ratio of the low-order terms is

$$\frac{B_{j,0}}{A_{j,0}} = \frac{S_j}{C_j} = \frac{ie^{i\theta_j} \sin \phi_j/2}{\cos \phi_j/2}$$

where ϕ_j is the tip angle produced by this segment of the pulse, and θ_j is the RF phase. The rotation angle ϕ_j is then

$$\phi_j = 2 \tan^{-1} \left| \frac{B_{j,0}}{A_{j,0}} \right|$$

and the RF phase is

$$\theta_j = \angle(-iB_{j,0}/A_{j,0}).$$

The RF waveform is then

$$B_{1,j} = \frac{1}{\gamma \Delta t} \phi_j e^{i\theta_j}. \tag{16}$$

This expression for the RF coupled with the backward recursion of (15) constitute the inverse SLR transform.

Hence, there is a unique invertible transform relationship between an RF pulse and two polynomials $A_n(z)$ and $B_n(z)$

$$B_1(t) \overset{\mathfrak{SLR}}{\Leftrightarrow} (A_n(z), B_n(z)).$$

This transform relationship makes RF pulse design equivalent to the design of two complex polynomials. The design of these polynomials is the subject of the rest of this paper.

E. RF Pulse Design by Polynomial Design

There are several different approaches that can be taken in designing the polynomials $A_n(z)$ and $B_n(z)$. One approach [1], [2], [6], [7], [9] is to first approximate the magnetization component of interest with a polynomial, and then factor it according to the type of slice profile to solve for $A_n(z)$ and $B_n(z)$. The approach we will take here [7]–[9] uses the fact that $B_n(e^{i\gamma Gx\Delta t})$ is proportional to the sine of half the tip angle at position x (2). $B_n(z)$ is designed to optimally approximate the ideal slice profile. $A_n(z)$ is then calculated to be consistent with $B_n(z)$, subject to the additional constraint that the resulting RF pulse have minimum energy. Once $A_n(z)$ and $B_n(z)$ have been determined the RF pulse is found by the inverse SLR transform.

For the sake of concreteness assume we are designing a $\pi/2$ pulse about the x-axis. In this case the ideal $B_I(z)$ polynomial evaluated at $e^{i\gamma Gx\Delta t}$ is

$$B_I(e^{i\gamma Gx\Delta t}) = i(n_x + in_y) \sin \phi(x)/2 = i \sin \phi(x)/2$$

since $\boldsymbol{n} = (1, 0, 0)^T$. In-slice this is

$$B_I(e^{i\gamma Gx\Delta t}) = i \sin \pi/4 = i\sqrt{2}/2$$

while out-of-slice this is

$$B_I(e^{i\gamma Gx\Delta t}) = i \sin 0 = 0.$$

Given this ideal $B_I(z)$ we wish to find a polynomial approximation. There are many possible methods for designing this polynomial. One powerful method is the Parks–McClellan (PM) algorithm for the design of linear-phase finite impulse response (FIR) digital filters [19]. The algorithm requires the specification on the edges of the in-slice and out-of-slice regions, and the relative ripples in each. These can be calculated fairly exactly using the pulse design trade-off relationships that will be presented below. The ideal $B_I(z)$ and a polynomial approximation both evaluated along the unit circle $z = e^{i\gamma Gx\Delta t}$ are plotted in Fig. 2.

Given the $B_n(z)$ polynomial we need to find a consistent $A_n(z)$ polynomial. The constraint $\alpha\alpha^* + \beta\beta^* = 1$ means that the magnitude of the $A_n(z)$ polynomial is

$$|A_n(z)| = \sqrt{1 - B_n(z) B_n^*(z)} \tag{17}$$

again evaluated along the unit circle $z = e^{i\gamma Gx\Delta t}$. An additional constraint is required to make the choice of $A_n(z)$ unique. One possibility is to choose $A_n(z)$ to be a minimum-phase polynomial. As was mentioned in [7], a minimum phase $A_n(z)$ results in a minimum energy RF pulse.

The minimum-phase $A_n(z)$ is easily found by noting that a minimum-phase polynomial is an analytic signal [20]. Analytic signals have the property that their log-magnitude and phase are a Hilbert transform pair. Hence, the minimum-phase $A_n(z)$ is

$$A_n(z) = |A_n(z)| \exp\left[i\mathfrak{IC}\left\{\log |A_n(z)|\right\}\right]. \tag{18}$$

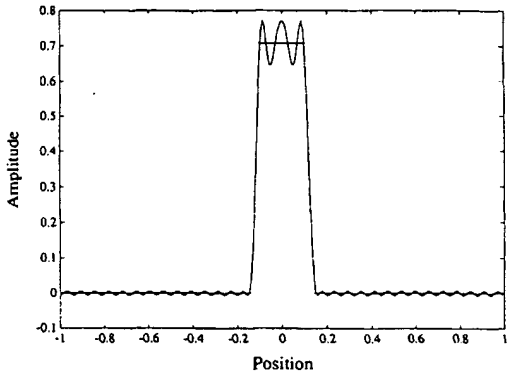

Fig. 2. Ideal $B_I(z)$ and the polynomial approximation produced by the PM algorithm.

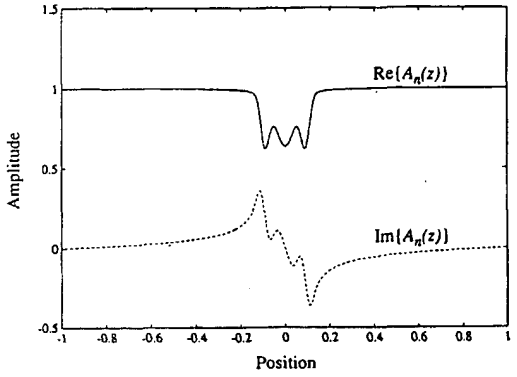

Fig. 3. Minimum-phase $A_n(z)$ corresponding to the $B_n(z)$ polynomial of Fig. 2.

Here $\mathcal{H}\{\cdot\}$ is the Hilbert transform operator. The PM algorithm gives the polynomial coefficients of $B_n(z)$. $B_n(z)$ must then be evaluated on the unit circle, which can be done with a DFT. The DFT order should be significantly larger than n to reduce aliasing errors in subsequent calculations. Once $B_n(z)$ has been calculated $|A_n(z)|$ can be found using (17). This is substituted into (18) to produce the minimum-phase polynomial $A_n(z)$ as evaluated along the unit circle. The polynomial coefficients are then found by an inverse DFT. Fig. 3 is a plot of the minimum-phase $A_n(z)$ as evaluated along the unit circle corresponding to the $B_n(z)$ of Fig. 2.

The reason the minimum-phase $A_n(z)$ corresponds to a minimum RF power is seen by examining the a_0 term of $A_n(z)$. From the forward recursion given in (13) it can be seen that a_0 has the simple form

$$a_0 = C_n C_{n-1} \cdots C_2 C_1$$

the product of the half angle cosines for all the incremental RF rotations. These incremental rotations are all small. Using the small angle approximation $\cos\theta/2 = 1 - \theta^2/8$ the product can be written

$$a_0 \approx (1 - \theta_n^2/8)(1 - \theta_{n-1}^2/8) \cdots (1 - \theta_2^2/8)(1 - \theta_1^2/8)$$

where $\theta_j = \gamma |B_{1,j}| \Delta t$. After multiplication the first two terms are

$$a_0 \approx 1 - \tfrac{1}{8} \sum_{j=0}^{n} \theta^2$$

$$= 1 - \tfrac{1}{8}(\gamma \Delta t)^2 \sum_{j=0}^{n} |B_{1,j}|^2. \qquad (19)$$

The second term is proportional to the pulse's average RF power. Hence, the pulse with minimum RF power has the maximum a_0. The polynomial with the maximum a_0 is the minimum-phase polynomial [20], [21].

The RF waveform computed by the inverse SLR transform of $A_n(z)$ and $B_n(z)$ is plotted in Fig. 4, and its slice profile in Fig. 5. Note that the ripples in-slice and out-of-slice are of constant amplitude, and that the slice is very well refocused. The M_x ripple is larger in-slice because ten times more ripple was allowed when the $B_n(z)$ polynomial was designed. The reason for this, and for choosing the width and location of the transition bands will be the subject of the next two sections.

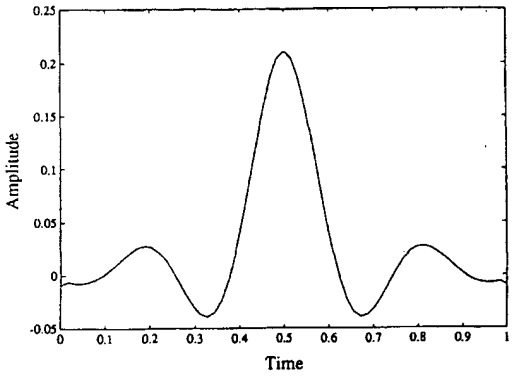

Fig. 4. SLR $\pi/2$ pulse corresponding to the $B_n(z)$ and $A_n(z)$ polynomials of Figs. 2 and 3.

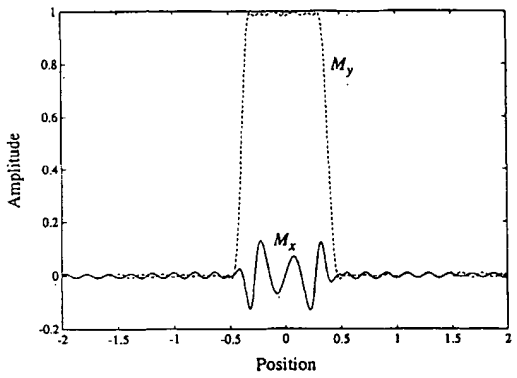

Fig. 5. Slice profile for the pulse plotted in Fig. 4.

III. Pulse Design Parameter Relations

The SLR algorithm reduces RF pulse design to the design of a single polynomial $B_n(z)$. The Parks-McClellan algorithm produces an optimal polynomial in the Chebyshev sense of minimizing the maximum ripple. As inputs it requires that the stopband and passband edges be specified, and that the relative ripple amplitudes in each of these bands be given. Pulse design

then consists of balancing the conflicting requirements for ripple, transition bandwidth, pulse length, slice width, and RF power.

The efficiency of the SLR algorithm allows RF pulses to be designed iteratively. The calculation of a 128 point $\pi/2$ pulse takes about 10 s on a Sun 3/50. Slice profile parameters can be iteratively optimized until a satisfactory design is achieved.

There is a better alternative. The characteristics of optimal FIR filters have been studied in detail [19]. Empirical relationships have been derived for the various filter design parameters. With some modification these relationships can be used to predict the attainable performance of RF pulses. Once a desired profile has been determined, the corresponding RF pulse is easily and rapidly computed.

The PM algorithm produces a linear-phase FIR filter. A linear-phase $\pi/2$ pulse can be refocused by a gradient reversal, and a linear-phase π pulse can be used as a spin-echo pulse. Optimal minimum-phase filters can be designed using the method described in [22], [23]. These have better performance, but at the cost of nonlinear phase response. When phase does not matter, as for selective inversion or saturation, the pulses based on minimum-phase filters will produce better slice profiles. Maximum-phase filters are also of interest. These are simply reversed minimum-phase filters.

A. Recasting the FIR Filter Parameter Relations

The parameter trade-offs for FIR filter design must be cast in a different form to be useful for the design of RF pulses. In particular the number of samples in the RF pulse is not ultimately significant, while the time-bandwidth product of the RF pulse is very important since it relates to the required RF power.

Fig. 6 illustrates the key parameters of the performance of an FIR filter. The parameter δ_1 is the amplitude of the passband ripple, δ_2 is the amplitude of the stopband ripple, F_p is the passband edge, and F_s is the stopband edge. The passband amplitude is unity, and all frequencies are normalized to the Nyquist frequency.

The empirical relationship between these parameters for an optimal FIR filter, such as is designed by the PM algorithm, is given by [19]

$$D_\infty(\delta_1, \delta_2) = (N - 1)\Delta F + f(\delta_1, \delta_2)(\Delta F)^2.$$

The parameter ΔF is the transition width $F_p - F_s$. The term $D_\infty(\delta_1, \delta_2)$ is an empirically derived performance measure of the filter. The term containing the $f(\delta_1, \delta_2)$ factor is negligible for almost any practical RF pulse, and will be dropped. The sample spacing is Δt, so the length of the pulse is $T = (N - 1)\Delta t$. The half-amplitude width of the filter is approximately the average of the stopband and passband widths

$$B = \frac{2F_s + 2F_p}{2\Delta t}.$$

If we define the fractional transition width as

$$W = \frac{F_p - F_s}{F_p + F_s}$$

the D_∞ equation may be simplified to

$$D_\infty(\delta_1, \delta_2) = TBW. \tag{20}$$

This is the key design equation. Using it, the slice width, transition width, pulse duration, and ripple amplitudes may all be traded off analytically. This expression also allows the pulse designer to exactly calculate the required inputs for the Park-McClellan algorithm to produce an RF pulse with a specific performance.

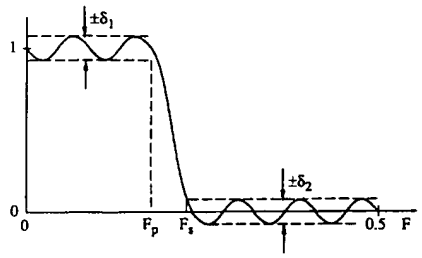

Fig. 6. Digital filter parameters.

The function D_∞ is an empirically derived performance measure for optimal FIR filters. For linear phase FIR filters it is given by [19]

$$D_{\infty,l}(\delta_1, \delta_2) = [a_1 L_1^2 + a_2 L_1 + a_3]L_2 + [a_4 L_1^2 + a_4 L_1 + a_6] \tag{21}$$

where $L_1 = \log_{10}\delta_1$, $L_2 = \log_{10}\delta_2$, and the a_i's are the coefficients

$$a_1 = 5.309 \times 10^{-3} \qquad a_4 = -2.66 \times 10^{-3}$$
$$a_2 = 7.114 \times 10^{-2} \qquad a_5 = -5.941 \times 10^{-1}$$
$$a_3 = -4.761 \times 10^{-1} \qquad a_6 = -4.278 \times 10^{-1}.$$

Fig. 7 is a plot of the linear-phase D_∞ as a function of δ_2 for a range of values for δ_1.

Minimum-phase FIR filters are easily designed using the method described in [22], [23]. If a minimum-phase filter of length N with ripple amplitudes δ_1 and δ_2 is desired, the PM algorithm is first used to design a linear-phase filter of length $2N - 1$ with ripple amplitudes $2\delta_1$ and $\delta_2^2/2$. If the frequency response of this linear-phase filter is biased up so as to be always positive, the result is the magnitude response squared of a minimum-phase filter. The minimum-phase filter is then computed by taking the square root to get the magnitude response, and then computing the corresponding minimum-phase polynomial as in (18). This filter will be of length N, and have ripple amplitudes δ_1 and δ_2.

This minimum-phase filter design method performs the same operations as required in [6] to design $B_n(z)$ by factoring M_z. It provides a direct way to compute one such factorization. In this case the method we use here of initially designing $B_n(z)$ produces one of the same pulses that is obtained by initially designing M_z and factoring.

The same basic design relation of (20) still holds for minimum-phase filters provided the correct expression for D_∞ is used. $D_{\infty,m}$ for optimal minimum-phase equal-ripple filters is given in terms of that for linear-phase filters by the expression

$$D_{\infty,m}(\delta_1, \delta_2) = \tfrac{1}{2} D_{\infty,l}(2\delta_1, \delta_2^2/2). \tag{22}$$

For most filters we will be concerned with (ripples of a few percent or less), the difference between $D_{\infty,l}$ and $D_{\infty,m}$ is on the order of 10–30%. This means that the minimum-phase filter can have a 10–30% narrower transition band, which is not a tremendous difference. However, for the same transition width the

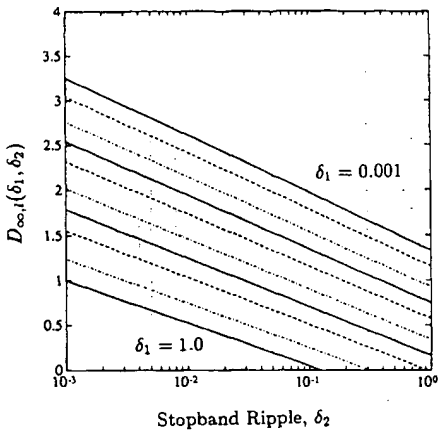

Fig. 7. $D_{\infty,1}$ as a function of out-of-slice ripple. Each plot corresponds to a different value of the in-slice ripple, starting at 0.001 for the top plot and going to 1.0 for the bottom plot. Plots corresponding to 0.001, 0.01, 0.1, and 1 are solid, 0.002, 0.02, and 0.2 are dashed, and 0.005, 0.05, and 0.5 are dot-dashed.

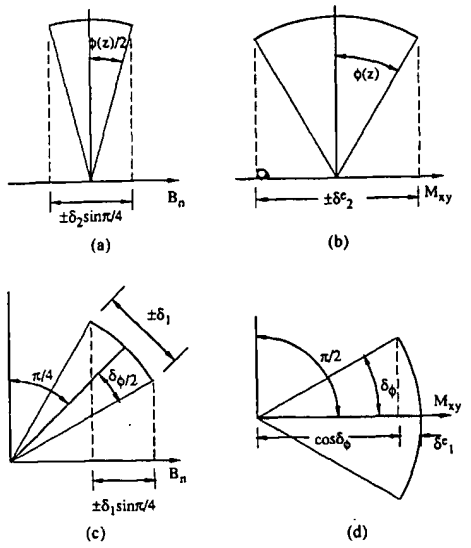

Fig. 8. Ripple geometry for $\pi/2$ pulse. The out-of-slice ripple geometry is illustrated in (a) and (b). (a) is the half-angle or spin-domain geometry, while (b) is the full-angle or magnetization space geometry. The in-slice half-angle and full-angle ripple geometries are shown in (c) and (d).

minimum-phase filter passband ripple can be smaller by a factor of four or more. This is a significant difference.

The design relation given in (20) describes the $B_n(z)$ polynomial. Unfortunately the relationship is generally nonlinear between the parameters of the $B_n(z)$ polynomial and the relevant feature of the slice profile. The nonlinearity is due to the geometry of the relationship between the $B_n(z)$ polynomial and the parameter of interest. Its effect is primarily in ripple amplitudes. We define the effective ripple amplitudes δ_1^e and δ_2^e as the ripple actually produced in the magnetization component of interest relative to the maximum value of the profile. For example, for a $\pi/2$ pulse δ_1^e and δ_2^e are the in-slice and out-of-slice ripples in M_{xy} relative to M_0. The δ_1 and δ_2 specified in the PM algorithm result in a slice profile with effective ripple amplitudes δ_1^e and δ_2^e. If the relationship between the specified polynomial ripple and effective slice profile ripple is known, we can calculate the ripple amplitudes to specify (δ_1 and δ_2) in order to get the effective ripple amplitudes that we would like (δ_1^e and δ_2^e). We will derive these relationships for five different types of pulses: small-tip-angle and $\pi/2$ excitation pulses, inversion pulses, crushed spin-echo pulses, and saturation pulses.

B. Small-Tip-Angle Pulses

The small-tip-angle case is the simplest. Here the initial magnetization lies along the z axis, and the parameter of interest is the transverse magnetization. In the small-tip-angle regime the RF pulse is proportional to the $B_n(z)$ polynomial, and the slice profile is proportional to the Fourier transform of the pulse. No compensation is required, so the specified and effective ripple amplitudes are the same

$$\delta_1 = \delta_1^e$$

$$\delta_2 = \delta_2^e.$$

C. $\pi/2$ Pulses

The next case is of $\pi/2$ selective excitation pulses. Here there is considerable geometric distortion between the ripple as specified by the $B_n(z)$ polynomial and the ripple in the resulting slice profile. To calculate the effective δ_1^e and δ_2^e we will assume that the $B_n(z)$ polynomial evaluated along the unit circle is

$$B_n(e^{i\gamma G x \Delta t}) \simeq \sin \phi(x)/2$$

where $\phi(x)$ is the tip angle at a position x.

The out-of-slice ripple is in the small-tip-angle regime. From Fig. 8(a) it can be seen that for z corresponding to a ripple peak

$$\delta_2 \sin\frac{\pi}{4} \simeq \sin \phi(x)/2.$$

The $\sin(\pi/4)$ factor scales the polynomial to the proper in-slice value for a $\pi/2$ pulse. The effective ripple is illustrated in Fig. 8(b), and can be calculated as

$$\begin{aligned}\delta_2^e &= \sin \phi(x) \\ &\simeq 2 \sin \phi(x)/2 \\ &= 2\delta_2 \frac{\sqrt{2}}{2} \\ &= \sqrt{2}\delta_2.\end{aligned}$$

The polynomial ripple that corresponds to a given effective ripple is then

$$\delta_2 = \delta_2^e/\sqrt{2}.$$

In-slice the $\mathcal{B}_n(z)$ polynomial is bounded by $(1 \pm \delta_1)$ $\sin(\pi/4)$. At an in-slice ripple peak

$$B_n(e^{i\gamma G x \Delta t}) = \sin \phi(x)/2$$

$$(1 \pm \delta_1) \sin\frac{\pi}{4} = \sin \phi(x)/2.$$

This is illustrated in Fig. 8(c). From the figure we deduce

$$\phi(x) \simeq \pi/2 \pm 2\delta_1.$$

The effective ripple is the variation in M_{xy} produced by the $2\delta_1$ ripple in $\phi(x)$. The effective ripple δ_1', shown in Fig. 8(d), can then be approximated as

$$\begin{aligned}\delta_1' &\simeq 1 - \cos 2\delta_1 \\ &\simeq 1 - \left(1 - \tfrac{1}{2}(2\delta_1)^2\right) \\ &= 2\delta_1^2.\end{aligned}$$

Note that the ripple is no longer symmetric about the desired value. The filter passband had a tolerance of $\pm\delta_1$ while the slice profile has a tolerance of $+0$, $-2\delta_1^2$. The polynomial ripple corresponding to a given effective ripple is

$$\delta_1 = \sqrt{\delta_1'/2}.$$

D. Inversion Pulses

For inversion pulses the parameter of interest is M_z. The major change in the analysis for π pulses is that the $B_n(z)$ polynomial is constrained to be less than one. The polynomial produced by the PM algorithm has a value of $1 \pm \delta_1$ in the passband. This is scaled so that the passband is bounded by $(1 - \delta_1) \pm \delta_1$.

From (6) the inversion pulse slice profile is given by

$$M_z^+ = (\alpha\alpha^* - \beta\beta^*)M_0.$$

Using the constraint that $\alpha\alpha^* + \beta\beta^* = 1$, this equation can be reduced to a function of β only

$$M_z^+ = (1 - 2\beta\beta^*)M_0. \tag{23}$$

An out-of-slice ripple of δ_2 in the $B_n(z)$ polynomial produces a ripple

$$\delta_2' = 2\delta_2^2$$

in the out-of-slice M_z^+ profile. The polynomial ripple corresponding to a given effective ripple is then

$$\delta_2 = \sqrt{\delta_2'/2}.$$

In-slice $B_n(z)$ goes from $(1 - 2\delta_1)$ to 1. The maximum in-slice ripple occurs when $B_n(z)$ is a minimum

$$\begin{aligned}M_z^+ &= \left(1 - 2(1 - 2\delta_1)^2\right)M_0 \\ &= (1 - 2 + 8\delta_1 - 8\delta_1^2)M_0 \\ &\simeq -1 + 8\delta_1.\end{aligned}$$

The effective ripple is then

$$\delta_1' = 8\delta_1$$

and the polynomial ripple for a given effective ripple is

$$\delta_1 = \delta_1'/8.$$

E. Crushed Spin-Echo Pulses

The case of a spin-echo pulse surrounded by dephasing, or crusher, gradients is of considerable practical interest. The magnetization is initially in the transverse plane, and the parameter of interest is the resulting M_{xy}.

From (10) the transverse magnetization produced by a crushed spin-echo RF pulse is

$$M_{xy} = i\beta^2 M_0$$

for an initial magnetization is along the $+y$ axis. The effective out-of-slice ripple is then

$$\delta_2' = \delta_2^2$$

which may be inverted to give

$$\delta_2 = \sqrt{\delta_2'}.$$

The $B_n(z)$ polynomial is scaled to be less than one, as it was for inversion pulses. In-slice the polynomial is bounded by $(1 - \delta_1) \pm \delta_1$, so the effective ripple is

$$\begin{aligned}\delta_1' &= 1 - (1 - 2\delta_1)^2 \\ &\simeq 4\delta_1.\end{aligned}$$

Solving for δ_1 as a function of δ_1',

$$\delta_1 = \delta_1'/4.$$

F. Saturation Pulses

Saturation technically means the destruction of the sample's net magnetization. It is then no longer able to produce a signal until the magnetization recovers. What we are actually referring to here are $\pi/2$ excitation pulses followed by a large dephasing gradient. This suppresses the signal produced by the magnetization in a slice, but does not destroy it. For example, it can still produce a stimulated echo. The term "suppression pulses" would be more accurate, but the term "saturation pulses" is now well entrenched.

The important magnetization component for saturation pulses is M_z. After the saturation pulse all transverse magnetization is assumed to be dephased. The saturated magnetization should be left with no M_z so that subsequent excitation pulses will produce no signal. The unsaturated magnetization should be left with its full M_z so that when subsequently excited it will produce its full signal.

The saturation pulse profile is given by the same expression as for the inversion profile, given in (23)

$$M_z^+ = (1 - 2\beta\beta^*)M_0.$$

The difference is in the scale factor for the β polynomial, and this changes the nature of the geometry. A saturation pulse is basically a $\pi/2$ pulse, so that the β polynomial is the PM polynomial scaled to $\sin \pi/4 = \sqrt{2}/2$.

Out-of-slice the polynomial ripple is $\pm\delta_2\sqrt{2}/2$, so that the out-of-slice M_z ripple is

$$\begin{aligned}M_z^+ &= (1 - 2\beta\beta^*)M_0 \\ &= \left(1 - 2(\delta_2\sqrt{2}/2)^2\right)M_0 \\ &= (1 - \delta_2^2)M_0.\end{aligned}$$

The effective ripple is then

$$\delta_2' = \delta_2^2$$

which can be inverted to give

$$\delta_2 = \sqrt{\delta_2'}.$$

In-slice the polynomial ripple is bounded by $(1 \pm \delta_1)\sqrt{2}/2$, so the in-slice M_z is bounded by

$$\begin{aligned}M_z^+ &= (1 - 2\beta\beta^*)M_0 \\ &= \left(1 - (1 \pm \delta_1)^2\right)M_0 \\ &\simeq \mp 2\delta_1 M_0.\end{aligned}$$

TABLE I
PARAMETER RELATIONS FOR VARIOUS RF PULSES

Case	δ_1	δ_2
Small-Tip	δ_1^e	δ_2^e
$\pi/2$	$\sqrt{\delta_1^e/2}$	$\delta_2^e/\sqrt{2}$
Inversion	$\delta_1^e/8$	$\sqrt{\delta_2^e/2}$
Spin-Echo	$\delta_1^e/4$	$\sqrt{\delta_2^e}$
Saturation	$\delta_1^e/2$	$\sqrt{\delta_2^e}$

The effective ripple is then

$$\delta_1^e = 2\delta_1$$

so the polynomial ripple for a given effective ripple is

$$\delta_1 = \delta_1^e/2.$$

G. Summary

This section has been largely concerned with determining the relationship between the ripple in $B_n(z)$ and the effective ripple in the magnetic resonance parameter of interest. For convenience the key results are summarized in Table I.

IV. Design Examples

We next present several examples of how the results of the previous section are used to design pulses. The design relations first allow the pulse designer to trade off parameter values analytically. Then when an acceptable set of parameters has been selected, the relations tell exactly how to design the pulse that meets the predicted performance.

A. Linear-Phase $\pi/2$ Pulses

The first example is the design of slice-selective $\pi/2$ pulses. These are a principal component of most imaging pulse sequences. This case will be examined in some detail both to illustrate the design method, and to show the nature of the design trade-offs.

Usually we would like the excited slice to be refocused by a reversal of the slice select gradient. This can be assured by using a linear-phase $B_n(z)$ polynomial. Most of the pulses we will present in this section will be linear-phase, and hence refocusable. Refocusing is not always required, though. An example is a field-of-view restriction pulse, like the slab-select pulse used in 3-D imaging. The phase profile of the slab is resolved by the imaging gradients. The phase is then suppressed by magnitude detection. When refocusing is not required significant advantages can be obtained by using a minimum-phase pulse. These include improved slice profile and reduced flow artifacts. An example of such a pulse is presented in the next section.

We would like to produce a 0.5 cm thick slice with a pulse duration of 4.0 ms. If the gradient system can produce a maximum gradient strength of 1 G/cm, the bandwidth of the pulse must be

$$\begin{aligned} B &= \gamma G \Delta x \\ &= (4.26 \text{ kHz/G})(1 \text{ G/cm})(0.5 \text{ cm}) \\ &= 2.13 \text{ kHz}. \end{aligned}$$

The time-bandwidth product is then

$$\begin{aligned} TB &= (4 \text{ ms})\,(2.13 \text{ kHz}) \\ &= 8.52. \end{aligned}$$

For convenience we will assume that the time-bandwidth product we are designing to is 8. The resulting pulses will produce 0.47 cm slices at full gradient amplitude, or will produce 0.5 cm slices at a gradient amplitude of 0.94 G/cm.

The remaining design parameters are the in-slice and out-of-slice ripple amplitudes, and the width of the transition band. Choosing any two of these determines the third. Here we choose the two ripple amplitudes and then solve for the required fractional transition width using (20). We could just as well choose the transition width and use (20) to solve for D_∞, and then pick two ripple amplitudes that will produce that D_∞.

We also have to decide how many samples to use for the RF pulse. Fewer samples result in faster execution of the pulse algorithm. It also produces larger tip angles for each sample in the RF pulse, and this can result in the hard-pulse approximation being violated. The number of points only has to be sufficient so that the slice-profile ripples are greater than the errors introduced by the hard-pulse approximation. Higher quality slice profiles require finer sampling. The effect of inadequate sampling is usually most noticable as nonequal out-of-slice ripple. For the examples presented in this section 65 samples are used for the RF waveform, which results in a maximum tip angle of 12° per sample for pulses with a time-bandwidth product of 8.

The other consideration for choosing the number of samples is that the sampling of the RF waveform will also excite sidelobes at multiples of the RF sampling frequency. The location and shape of these sidelobes can be calculated by a Fourier analysis since the sidelobe tip angles will be small. These sidelobes may be pushed further out either by interpolating the RF waveform as in [6], or by interpolating the $B_n(z)$ polynomial before the inverse SLR transform. The latter approach has the added benefit of reducing the errors in the hard-pulse approximation, resulting in more accurate RF pulses. Increasing the filter order used for $B_n(z)$ is effectively just an interpolation method.

Solving (20) for the fractional transition width

$$W = \frac{D_\infty}{TB}.$$

As a first example let the in-slice ripple and the out-of-slice ripple both be 1%. Using the expressions from Table I the required polynomial ripples are $\delta_1 = 7.1\%$ and $\delta_2 = 0.71\%$. These values are then substituted into the linear-phase D_∞ expression (21) to give

$$D_{\infty,l} = 1.44.$$

The fractional transition width is then

$$W = \frac{1.44}{8} = 0.18.$$

The PM algorithm requires the location of the edges of the stop and passbands relative to the sampling frequency. If the RF pulse has 65 samples over 4 ms, the sampling frequency is 16 kHz. The slice is 2 kHz in width, so it extends from ±1 kHz. The transition band is

$$BW = (2 \text{ kHz})(0.18) = 0.36 \text{ kHz}.$$

This puts the passband edge at $(1 - 0.36/2) = 0.82$ kHz and the stopband edge at $(1 + 0.36/2) = 1.18$ kHz. Normalizing by the sampling frequency

$$F_p = 0.82/16 = 0.05125$$

$$F_s = 1.18/16 = 0.07375.$$

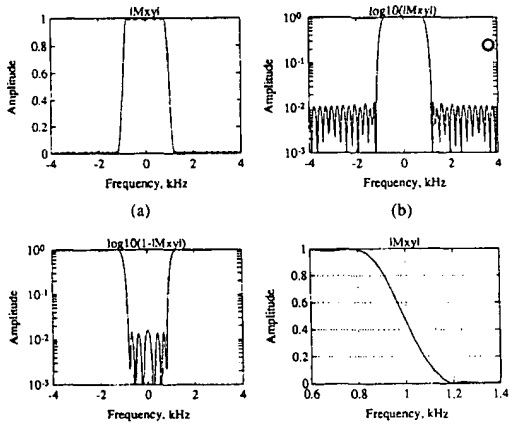

Fig. 9. The performance of the 1% ripple $\pi/2$ pulse. Plot (a) shows $|M_{xy}|$, while (b) is the same plot on a log scale. This shows that the out-of-slice ripple is close to the design value of 1%. Plot (c) is of $1 - \log_{10}|M_{xy}|$ which shows the in-slice ripple. It is also close to its 1% design value. Plot (d) shows that the transition band is approximately the specified 360 Hz, and that the half amplitude point falls close to the intended 1 kHz.

The only remaining input for the PM algorithm is the weighting of the in-slice and out-of-slice ripples. The in-slice ripple should be weighted by $1/\delta_1$ and the out-of-slice ripple by $1/\delta_2$.

The RF pulse that results from these specifications is that plotted previously in Fig. 4. The performance of this RF pulse is shown in Fig. 9. Fig. 9(a) is the absolute value of the slice profile. Fig. 9(b) is the same plot on a log scale. The out-of-slice ripple is close to the design value of 1%. Fig. 9(c) is a plot of $1 - \log_{10}|M_{xy}|$. This shows that the in-slice ripple is also close to its design value of 1%, although again it is exceeded slightly. Fig. 9(d) shows that the transition width is approximately the desired value of 360 Hz, and that the half amplitude point falls close to the intended 1 kHz. The transition width can be increased slightly if it is critical to achieve the specified ripple amplitudes exactly.

Figs. 10 and 11 compare this SLR pulse to a Hamming windowed sinc pulse, such as is commonly used on commercial imaging systems. Although the RF pulses are similar in character there are several differences in the slice profiles. The SLR pulse has uniform ripple both in-slice and out-of-slice. The Hamming windowed sinc has very little ripple in-slice, and only one significant sidelobe out-of-slice. The amplitude of this sidelobe is about 5%. The transition width of the windowed sinc is 50% wider than that of the SLR pulse. The SLR pulse would be preferable in cases where adjacent slices are being excited, such as multislice imaging. Both the absence of the sidelobe and the sharper profile reduce crosstalk between slices.

In the previous example we simply chose the in-slice and out-of-slice ripple to be 1%. This determined the transition width. An important design trade-off is the relationship between the ripple amplitudes and the transition width. A large reduction in ripple amplitude can be obtained with a relatively small increase in transition width. Fig. 12 is a plot of two SLR pulses designed with 5% and 0.2% in-slice and out-of-slice ripple amplitudes. Fig. 13 is a plot of the slice profiles produced by these pulses. The ripple amplitude has been reduced by a factor of 25 at a cost of a factor of 2.5 in transition width. This overstates the difference in transition widths. If the same 5% ripple criteria

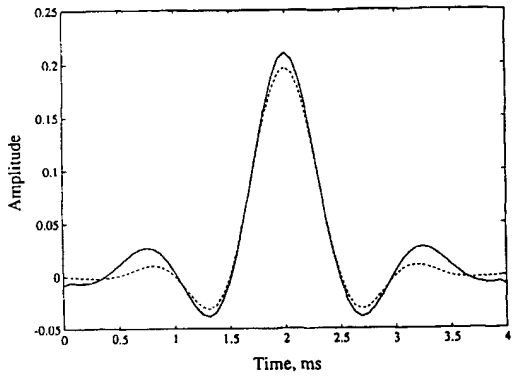

Fig. 10. Comparison of the SLR 1% ripple pulse (solid line) to a Hamming windowed sinc pulse (dashed line).

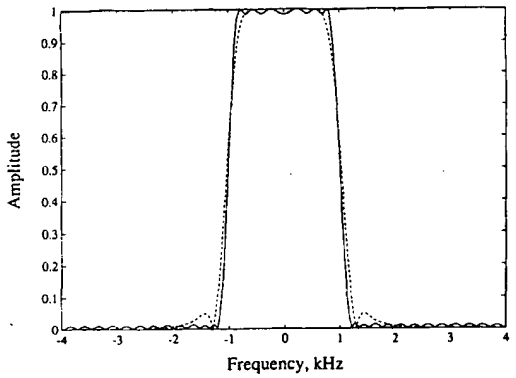

Fig. 11. Slice profiles produced by the SLR 1% ripple pulse (solid line) and the Hamming windowed sinc pulse (dashed line).

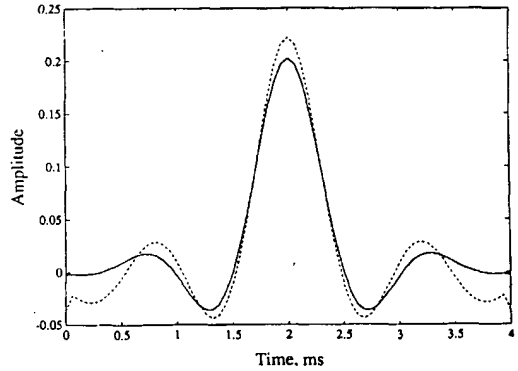

Fig. 12. SLR pulses with ripple amplitudes of 5% (solid line) and 0.2% (dashed line).

are used to measure both transition widths, the increase is less than a factor of 2. A very large reduction in ripple is obtained with a moderate reduction in slice sharpness.

B. Minimum-Phase $\pi/2$ Pulses

Linear-phase pulses are not always required or desirable. One example is a field-of-view restriction pulse. Here the slice will

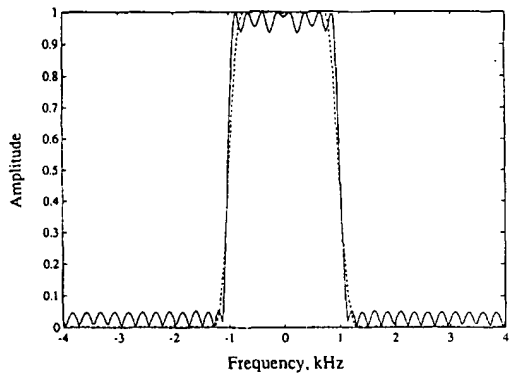

Fig. 13. Slice profiles produced by the 5% ripple (solid line) and 0.2% ripple (dashed line) SLR pulses.

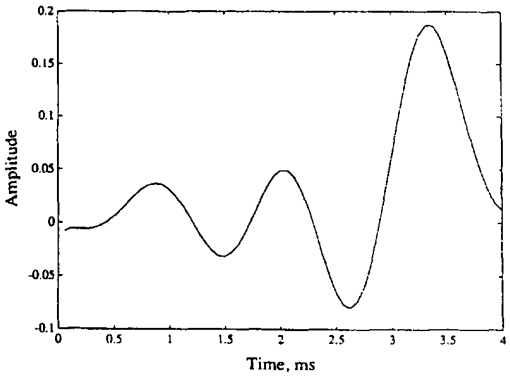

Fig. 14. Minimum-phase $\pi/2$ pulse.

be resolved by the imaging gradients, so the phase across the slice is unimportant provided it is small across a voxel. Nishimura *et al.* showed that an off-center RF pulse produces significantly less flow dephasing than a linear-phase pulse, with only a minor penalty in slice profile [24]. A minimum-phase pulse obtains a similar reduction in flow dephasing along with an improvement in slice profile.

The minimum-phase pulse requires a maximum-phase filter because the filter phase is relative to its first sample, while the phase produced by the pulse is relative to its last sample. The maximum-phase filter is simply the minimum-phase filter reversed.

The minimum-phase pulse will have essentially the same integrated RF power as the corresponding linear-phase pulse. Both have similar $|B_n(z)|$ profiles as evaluated along the unit circle, so both will have essentially the same $A_n(z)$ polynomials. From (19), both pulses will have the same integrated RF power.

The higher performance of the minimum-phase filters can be used to improve any combination of the slice-profile parameters. If we again specify in-slice and out-of-slice ripple amplitudes at 1% the minimum-phase $D_{\infty,m}$ may be calculated from (22) to be 1.26. This is smaller than the 1.44 for the linear-phase pulse. The reduction in D_∞ can be used to reduce any term in the product *TBW*. For example, the transition width W can be reduced by 15% to 300 Hz. This is 60 Hz less than for the linear-phase pulse. The RF waveform and the simulated slice profile are plotted in Figs. 14 and 15. The slice profile is shown

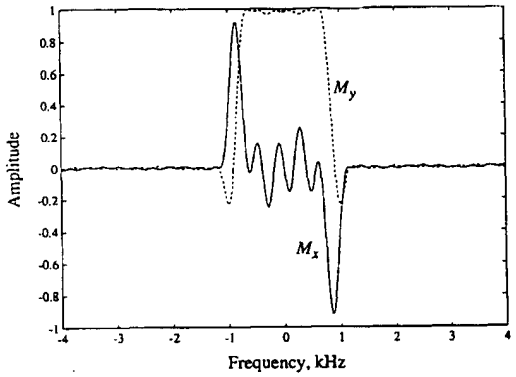

Fig. 15. Refocused minimum-phase slice profile. The refocusing gradient lobe is 0.16 times the slice-select gradient area.

refocused by a gradient area of only 0.16 times the slice select gradient area. In comparison a linear-phase pulse requires a refocusing gradient area of 0.5 times the slice select gradient area.

Rather than reducing one of the terms in the *TBW* product, we could also choose smaller ripple amplitudes so that $D_{\infty,m}$ is the same as $D_{\infty,l}$ for the 1% ripple linear-phase pulse. Two possibilities are reducing the out-of-slice ripple by a factor of two, or reducing the in-slice ripple by a factor of five.

C. π Inversion and Spin-Echo Pulses

The same basic design method can be used to design inversion and spin-echo pulses. The only difference is which expression from Table I is used to compute the polynomial ripple required to produce the desired effective ripple. The computed polynomial ripple is then used to compute D_∞.

The example presented in this section has the same bandwidth and duration as the $\pi/2$ pulse of the previous section, 2 kHz and 4 ms, respectively. The time-bandwidth product is again 8. The design is of an inversion pulse with 1% ripple in-slice and out-of-slice. Since we do not care about phase for an inversion pulse we can use either a linear-phase or minimum-phase pulse.

For the linear-phase case the corresponding $D_{\infty,l}$ is 2. The fractional transition width is $2/8 = 0.25$, for a transition width of 500 Hz. The transition band then extends from 750 Hz to 1.25 kHz. The number of points used in the design is 128 to ensure that the hard-pulse approximation is satisfied. The resulting pulse and its slice profile are shown as the solid lines in Figs. 16 and 17. The slice profile actually has slightly less ripple than specified. The in-slice and out-of-slice ripple are both about 0.8%.

Note that the pulse has two large values at either end of the pulse. These are due to the fact that a significant out-of-slice ripple in the spectrum of the pulse produces very little out-of-slice ripple in the M_z component. This ripple allows a narrower transition width to be obtained. These are known in our group as "Conolly wings" because they appeared frequently in Conolly's optimized inversion pulses [15].

For the minimum-phase case the $D_{\infty,m}$ is 1.36, which is significantly less than for the linear-phase pulse. The transition width is then reduced to 340 Hz. The minimum-phase pulse and its slice profile are plotted as the dashed lines in Figs. 16 and 17. The ripple amplitudes are almost exactly the designed 1% values.

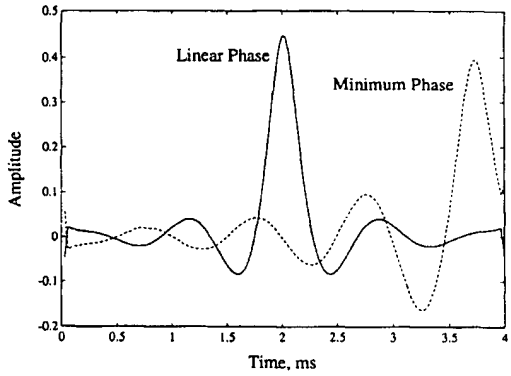

Fig. 16. SLR inversion pulses designed to have a 1% ripple both in-slice and out-of-slice. The solid line is a linear-phase pulse, and the dashed line is a minimum-phase pulse.

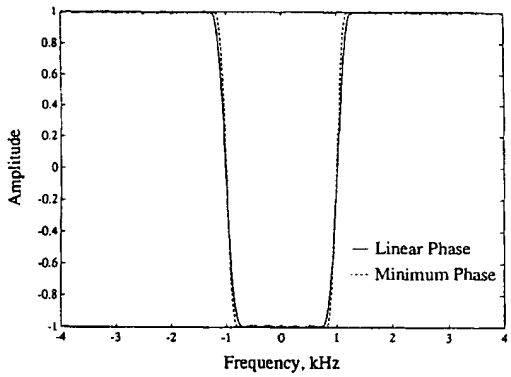

Fig. 17. M_z produced by the 1% ripple SLR inversion pulses of Fig. 16.

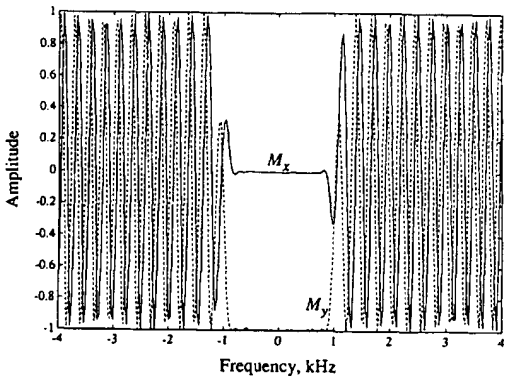

Fig. 18. Spin-echo profile produced by the linear-phase pulse of Fig. 16 used without surrounding crusher gradients.

The linear-phase pulse can also be used as a spin-echo pulse. The spin-echo slice profile produced by this pulse without surrounding crusher gradients is plotted in Fig. 18. The slice profile with surrounding crusher gradients is plotted in Fig. 19. In both cases the phase across the slice is very flat. The ripple is

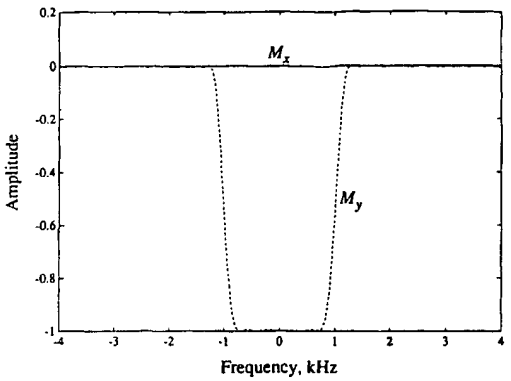

Fig. 19. Spin-echo profile produced by the linear-phase pulse of Fig. 16 used with crusher gradients.

less than for the inversion profile, as would be expected from a comparison of the entries in Table I.

In [6] it is noted that an inversion pulse can have half the transition width of a spin-echo pulse of the same duration. Here this is reflected in the difference between $D_{\infty,I}$ for the refocusing pulse and $D_{\infty,m}$ for the minimum-phase pulse. This difference depends on the number of passband zeros in the $B_n(z)$ polynomial [22]. For a very narrow slice with no passband zeros (a single lobe RF pulse) the minimum-phase and linear-phase pulses are identical. For a wide passband with many passband zeros the 2 to 1 ratio noted in [6] can be approached. For the examples shown in this section the minimum-phase inversion pulse has a transition width that is $340/500 = 0.68$ times that of the linear-phase pulse.

The design of π pulses is probably the most important application of the SLR algorithm. Fourier methods fail badly in the design of pulses with tip angles of this size. Optimization methods are capable of designing good π pulses, but require considerably more time and computation. The SLR algorithm makes the design of π pulses quick, and it analytically predicts the attainable slice profile.

D. Saturation Pulses

An ideal saturation pulse would leave no M_z magnetization for the saturated spins. In practice the effectiveness of a saturation pulse is determined primarily by the RF uniformity across the subject. On our 1.5T GE Signa System the subject induced variation is on the order of 10%. The saturation pulse in-slice ripple should be somewhat less than this so that RF uniformity is the performance limiting factor. The out-of-slice ripple can easily be made quite small due to the square dependence of the M_z ripple on the polynomial ripple.

As an example we again consider a 4 ms, 2 kHz bandwidth pulse. Since the slice will not be refocused we do not need a linear-phase pulse. The excited magnetization will be suppressed by a subsequent dephasing gradient anyway, so it is advantageous for the excitation pulse to leave the slice with as much phase as possible. This is accomplished by using a maximum-phase pulse, which is based on a minimum-phase $B_n(z)$.

If we specify the in-slice ripple as 1% and the out-of-slice ripple as 0.1%, we calculate D_∞ to be about 1.36. This gives a fractional transition width of 0.17, or a transition width of 340

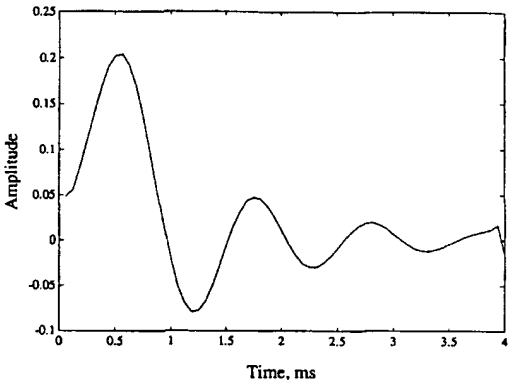

Fig. 20. Maximum-phase saturation pulse.

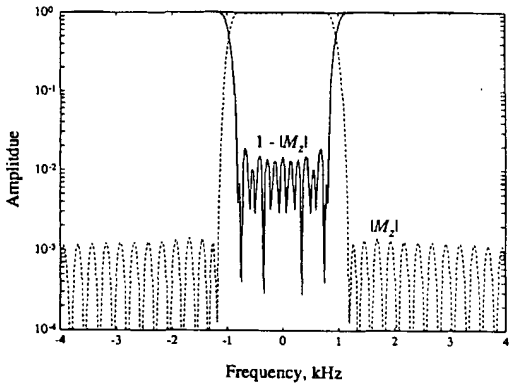

Fig. 21. Log-magnitude slice profile for the saturation pulse of Fig. 20.

Hz. The resulting pulse is shown in Fig. 20, and a log plot of the slice profile is shown in Fig. 21.

V. Conclusion

This paper has outlined the Shinnar–Le Roux algorithm for the design of RF pulses. Beyond its inherent speed, perhaps its most useful feature is that slice profiles can be predicted analytically. Slice profile parameters can be traded off before ever designing a pulse. This allows RF pulse design to be fully integrated into pulse sequence design. A number of pulse designs were presented. These included the usual $\pi/2$ and π pulses used in most MR scanners, as well as a saturation pulse, and minimum-phase and maximum-phase pulses.

References

[1] M. Shinnar, L. Bolinger, and J. S. Leigh, "Use of finite impulse response filters in pulse design," in *Proc. 7th SMRM*, Aug. 1988, p. 695.
[2] M. Shinnar, L. Bolinger, and J. S. Leigh, "Synthesis of soft pulses with specified frequency responses," in *Proc. 7th SMRM*, Aug. 1988, p. 1040.
[3] M. Shinnar, S. Eleff, H. Subramanian, and J. S. Leigh, "The synthesis of pulse sequences yielding arbitrary magnetization vectors," *Magnet. Resonance Med.*, vol. 12, pp. 74–80, Oct. 1989.
[4] M. Shinnar, L. Bolinger, and J. S. Leigh, "The use of finite impulse response filters in pulse design," *Magnetic Resonance Med.*, vol. 12, pp. 75–87, Oct. 1989.
[5] ——, "The synthesis of soft pulses with a specified frequency response," *Magnet. Resonance Med.*, vol. 12, pp. 88–92, Oct. 1989.
[6] M. Shinnar and J. S. Leigh, "The application of spinors to pulse synthesis and analysis," *Magnet. Resonance Med.*, vol. 12, pp. 93–98, Oct. 1989.
[7] P. Le Roux, "Exact synthesis of radio frequency waveforms," in *Proc. 7th SMRM*, Aug. 1988, p. 1049.
[8] ——, "Simplified rf synthesis," in *Proc. 8th SMRM, Works in Progress*, Aug. 1989, p. 1168.
[9] ——, "French patent 8610179," 1986.
[10] W. S. Hinshaw and A. H. Lent, "An introduction to NMR imaging: From the Bloch equation to the imaging equation," *Proc. IEEE*, vol. 71, pp. 338–350, Mar. 1983.
[11] D. I. Hoult, "The solution of the Bloch equations in the presence of a varying B_1 field: An approach to selective pulse analysis," *J. Magnet. Resonance*, vol. 35, pp. 66–86, 1979.
[12] M. Silver, R. Joseph, and D. Hoult, "Selective pulse creation by inverse solution of the Bloch–Riccati equation," in *Proc. 2nd SMRM, Works in Progress*, Aug. 1983, p. 22.
[13] D. Lurie, "A systematic design procedure for selective pulses in NMR imaging," *Magnet. Resonance Imaging*, vol. 3, pp. 235–243, 1985.
[14] A. Lent and A. Kritzer, "A new RF pulse shape for narrow-band inversion: The WOW-180," in *Proc. 4th SMRM*, Aug. 1985, p. 1015.
[15] S. M. Conolly, D. G. Nishimura, and A. Macovski, "Optimal control solutions to the magnetic resonance selective excitation problem," *IEEE Trans. Med. Imaging*, vol. MI-5, pp. 106–115, 1986.
[16] J. B. Murdoch, A. H. Lent, and M. R. Kritzer, "Computer-optimized narrowband pulses for multislice imaging," *J. Magnet. Resonance*, vol. 74, pp. 226–263, 1987.
[17] E. T. Jaynes, "Matrix treatment of nuclear induction," *Phys. Rev.*, vol. 98, pp. 1099–1105, May 1955.
[18] V. H. Subramanian, S. M. Eleff, S. Rehn, and J. J. S. Leigh, "An exact synthesis procedure for frequency selective pulses," in *Proc. 4th SMRM*, Aug. 1985, pp. 1452–1453.
[19] L. R. Rabiner and B. Gold, *Theory and Application of Digital Signal Processing*. Englewood Cliffs, NJ: Prentice-Hall, 1975.
[20] A. Papoulis, *Signal Analysis*. New York: McGraw-Hill, 1977.
[21] A. V. Oppenheim and R. W. Schafer, *Digital Signal Processing*. Englewood Cliffs, NJ: Prentice-Hall, 1975.
[22] T. W. Parks and C. S. Burrus, *Digital Filter Design*. New York: Wiley, 1987.
[23] J. S. Lim and A. V. Oppenheim, *Advanced Topics in Signal Processing*. Englewood Cliffs, NJ: Prentice-Hall, 1987.
[24] D. G. Nishimura, A. Macovski, J. I. Jackson, R. S. Hu, C. A. Stevick, and L. Axel, "Magnetic resonance angiography by selective inversion recovery using a compact gradient echo sequence," *Magnet. Resonance Med.*, vol. 8, pp. 96–103, 1988.